PROCEEDINGS OF SCIENCE

The non-thermal core of 3C 111

Sandra de Jong*, **Volker Beckmann, Fabio Mattana**
François Arago Centre, APC, Université Paris Diderot, CNRS/IN2P3, CEA/Irfu, Obs. de Paris, Sorbonne Paris Cité, 10 Rue A. Domon et L. Duquet, 75205 Paris Cedex 13 - France
E-mail: dejong@apc.univ-paris7.fr

To shed light on the physical processes that can produce high-energy emission in non-blazar radio galaxy 3C 111 we analyzed both the X-ray spectrum from 0.4 to 200 keV and the spectral energy distribution of this source using archival and previously unpublished data. The combined X-ray spectra from *INTEGRAL*, *Swift* and *Suzaku* are well-represented by an absorbed exponentially cut off power law with reflection from neutral material with a photon index $\Gamma = 1.68 \pm 0.03$, a high-energy cut-off $E_{\rm cut} = 227^{+143}_{-67}$ keV, a reflection component with $R = 0.7 \pm 0.3$ and a Gaussian component to account for the iron emission line at 6.4 keV with an equivalent width of $EW = 86^{+18}_{-12}$ eV.

The data from *Suzaku*, *INTEGRAL*, *Swift* and *Fermi* in the X-ray to γ-ray regime, together with archival data in the radio, infrared, and optical band, can be modeled by a single-zone synchrotron self-Compton model without an additional thermal component.

We compare our model to the models for another radio galaxy, Cen A, and with a model for the blazar Mrk 421. The parameters which allow to model the spectral energy distribution in the three sources are consistent when considering the different jet power.

We suggest a hybrid model to explain the broad-band high-energy emission, including a thermal component (iron line, high-energy cut-off, reflection) and a non-thermal one (an additional thermal component to model the entire SED is not required).

The Extreme and Variable High Energy Sky
September 19-23, 2011
Chia Laguna (Cagliari) , Italy

*Speaker.

PoS(Extremesky 2011)076

1. Introduction

3C 111 is a nearby ($z = 0.049$) flat-spectrum FR-II radio galaxy. The source shows strong broad emission lines in the optical and an iron emission line in the X-ray regime, similar to Seyfert 1 galaxies. In the radio regime the emission is dominated by the synchrotron process in the relativistic jet, which has an angle of 18° to our line of sight [15]. The projected size of the jet is 78 kpc and there is no visible counter jet. A bright lobe is visible in the direction of a possible counter jet which is likely fed by the undetected counter jet [17]. The intrinsic absorption has a column density of $N_{\rm H} \simeq 7 \times 10^{21}\,{\rm cm}^{-2}$.

Recently it has been discovered that 3C 111, like several other non-blazar Active Galactic Nuclei (AGN), also emits in the γ-ray regime [1, 4, 14]. The second *Fermi*/LAT catalogue includes 11 associations with radio galaxies out of 1297 sources that have been identified. Although several explanations have been proposed (i.e., misaligned jet, shocks in the radio lobes) about the origins of this high-energy radiation, conclusive evidence for any of these hypotheses is yet to be found. By modeling the spectral energy distribution (SED) we study the processes responsible for the radiation at high energies of 3C 111.

2. Data analysis and results

INTEGRAL IBIS/ISGRI (20–1000 keV) has observed 3C 111 over several years for a total exposure time of 508 ks. In addition we used *Suzaku* XIS and PIN observations of 3C 111, in the energy ranges of $0.2-12\,{\rm keV}$ and $10-60\,{\rm keV}$, respectively, taken in August 2008 with a total duration of 237 ks. We added archival data from *Swift*/BAT (15–150 keV), using the 58 month hard X-ray survey from December 2004 to end of May 2009. We analyzed *Fermi*/LAT data above 100 MeV from observations between August 2008 and April 2011. Table 1 shows the results of the individual power-law fits to the data, with the photon index, model flux and used energy range. The results are obtained using XSPEC except for the *Fermi*/LAT data for which we used the maximum likelihood fit provided by `gtlike`.

We first fitted the X-ray spectrum only with an absorbed power law and a Gaussian component at 6.1 keV to account for the redshifted iron emission line. The fit resulted in $\chi^2_\nu = 1.24$ (1687 d.o.f.). We then applied a cut-off power law, which yielded a better fit with $\chi^2_\nu = 1.12$ (1686 d.o.f.), improving the null hypothesis probability by seven orders of magnitude. Adding a reflection component further improves the fit $\chi^2_\nu = 1.10$ (1676 d.o.f., ftest probability 3×10^{-32}). The resulting spectrum and residuals can be seen in Figure 1. The best-fit values and 90% errors are the intrinsic absorption $N_{\rm H} = (9.0 \pm 0.2) \times 10^{21}$ cm^{-2}, the photon index is $\Gamma = 1.68 \pm 0.03$, a high-energy cut-off at $E_{\rm cut} = 227^{+143}_{-67}\,{\rm keV}$, a reflection scaling factor $R = 0.7 \pm 0.3$ and an equivalent width of $EW = 86^{+18}_{-12}\,{\rm eV}$ of the iron line. It was not possible to fit the *Fermi*/LAT spectrum in XSPEC since the data yielded only two significant points, therefore we used the fit results from the instrument specific software (`gtlike`): a spectral slope of $\Gamma_\gamma = 2.4 \pm 0.2$ and a flux $f = 1.2 \times 10^{-8}\,{\rm ph\,cm^{-2}\,s^{-1}}$ (between 100 MeV–200 GeV).

We reconstructed the SED of 3C 111 combining our data with archival radio and (de-absorbed) infrared data from the NED and modeled this using the single-zone synchrotron self-Compton (SSC) code by Krawcynski et al. (2004) [19]. The SSC mechanism assumes an isotropic population

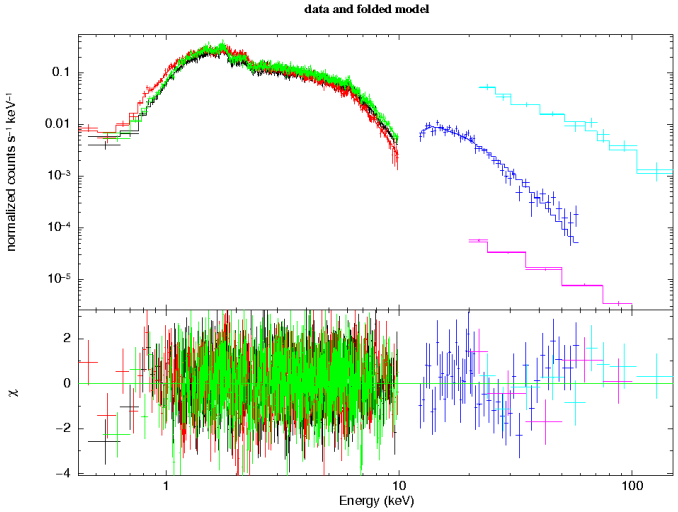

Figure 1: Count spectrum of the combined *Suzaku*/XIS, *Suzaku*/PIN, *INTEGRAL* IBIS/ISGRI and *Swift*/BAT data with the fitted model: an absorbed cut-off power law with reflection from neutron material and a Gaussian component to account for the iron Kα line at 6.4 keV (WABS*(PEXRAV+GAUSS)) . Below the residuals of the fit in units of standard deviations are shown.

Table 1: Indices for the individual power law fits to the data, and their 90% c.l. errors, the model flux and the energy range used. For the *Fermi*/LAT measurement we used the `gtlike` results.

Instrument	Γ	f [erg cm^{-2} s^{-1}]	Energy range
XIS0	1.60 ± 0.02	2.2×10^{-11}	0.4–10 keV
XIS1	1.59 ± 0.02	2.2×10^{-11}	0.4–10 keV
XIS3	1.63 ± 0.02	2.2×10^{-11}	0.4–10 keV
PIN	1.52 ± 0.14	4.8×10^{-11}	12–60 keV
ISGRI	1.9 ± 0.2	1.2×10^{-10}	20–200 keV
BAT	2.0 ± 0.1	1.1×10^{-10}	15–150 keV
LAT	2.4 ± 0.2	6.4×10^{-12}	$>$ 100 MeV

of high-energy electrons that emit synchrotron radiation followed by inverse Compton scattering of these photons to higher energies. The electron population is located in a spherical volume with radius R and a randomly oriented magnetic field B, that moves relativistically towards the observer with a bulk Lorentz factor γ, thus the radiation is Doppler-shifted with a Doppler factor δ. The electron energy spectrum in the jet-frame follows a broken power law, with indices p_1 and p_2, and is characterized by a minimum and a maximum energy ($E_{\rm min}$, $E_{\rm max}$) and a break energy $E_{\rm br}$. The values we used to model the data can be found in Table 2 and the resulting plot in Figure 2. The addition of an external Compton component does not improve the fit.

3. Discussion

We have constrained the high-energy cut-off of 3C 111 at $E_{\rm cut} = 227^{+143}_{-67}$ keV using the combined X-ray data. An indication for this cut-off can already be seen in the power law indices of

Table 2: Parameters to model the SED of 3C 111 using the Krawcynski code, compared with the parameters to fit the SED of the core of Cen A [2] and those to model the low state of Mrk 421 [9].

Parameter	Symbol	3C 111	Cen A	Mrk 421
δ	Doppler factor	13.9	1.0	10.0
R	Radius of the emission volume [cm]	2.0×10^{16}	3.0×10^{15}	7.0×10^{15}
B	Magnetic field of emission volume [G]	4×10^{-2}	6.2	0.405
$E_{\rm min}$	Minimum energy of the electron distribution [eV]	1.0×10^{7}	1.5×10^{8}	3.2×10^{6}
$E_{\rm max}$	Maximum energy of the electron distribution [eV]	7.1×10^{9}	5.0×10^{13}	1.7×10^{11}
$E_{\rm br}$	Break energy of the electron distribution [eV]	1.6×10^{9}	4.0×10^{8}	2.2×10^{10}
p_1	Electron spectral index ($E_{\rm min}$ to $E_{\rm br}$)	2.0	1.8	2.05
p_2	Electron spectral index ($E_{\rm br}$ to $E_{\rm max}$)	2.2	4.3	3.6
$\log L$	Bolometric Luminosity [erg s^{-1}]	44.4–45.2 [6]	43.6 [8]	45.5 [16]

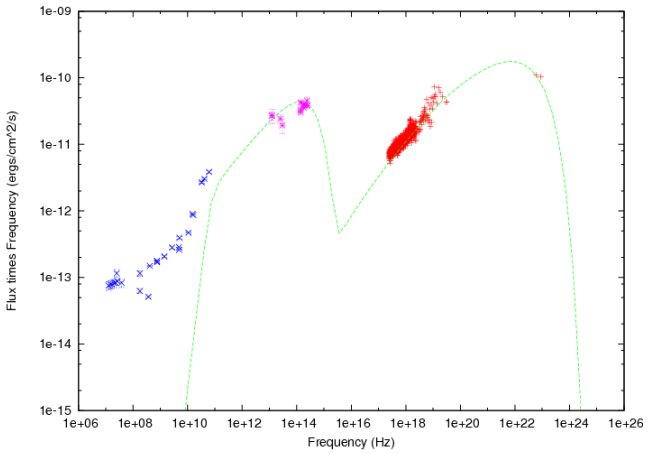

Figure 2: SED showing 3C 111 unabsorbed fluxes and the SSC one-zone model. Red crosses indicate data extracted and analyzed in this work. The purple stars are archival de-absorbed IR and the blue crosses archival radio data. The green line shows the SSC model. See Table 2 for the parameters applied.

the individual fits, which increase from $\Gamma\sim1.6$ in the soft X-ray band to $\Gamma\sim2$ in the hard band (Table 1). Our result is consistent with earlier findings of a lower limit of $E_{\rm cut}\geq82$ keV using *BeppoSAX* data [11], a lower limit on the cut-off of $E_{\rm cut}>75$ keV using data from *XMM-Newton*, *Swift* and *Suzaku* [6], and the measure of $E_{\rm cut}=126^{+193}_{-50}$ keV using *XMM-Newton*, *Swift* and *INTEGRAL* [20]. A high-energy cut-off is a property of the high-energy spectrum of Seyfert galaxies and the value we have found for 3C 111 is in the normal range for cut-off energies observed in Seyferts [7, 12].

The reflection scaling factor we found, $R=0.7\pm0.3$, is consistent with earlier findings $R=0.9\pm0.6$ [20]. The value we found is also consistent with general Seyfert properties; $R=1.2^{+0.6}_{-0.3}$ for Seyfert 1 and $R=1.1^{+0.7}_{-0.4}$ for Seyfert 2 galaxies [7].

The archival radio data used to model the SED are not well-represented by our SSC model. Since there is a large difference in the field of view probed by radio and X-ray observatories, it is possible we probe different regimes in the broad-band SED, which the one-zone model does not account for.

3C 111 has been suggested as a counterpart for the gamma-ray source 3EG J0416+3650 in the third *CGRO*/EGRET catalogue, however it fell outside of the 99% probability region [13]. A re-analysis of the data [21] concluded that 3EG J0416+3650 is likely associated with 3C 111. Indeed, there are no other plausible counterparts in the EGRET error region, which is also larger than previously thought [13] (the quoted errors were statistical only and did not take into account the larger systematic errors due to inaccuracies in the Galactic diffuse model). The EGRET data have been re-analyzed [14] and it has been found that 3EG J0416+3650 is likely to result from the blending of more than one source. One of these components (detected only above 1 GeV) can be associated with 3C 111. Furthermore 3C 111 was included in the first Fermi/LAT source catalogue [3] with a significance of 4.3σ. In the second *Fermi*/LAT source catalogue 3C 111 has been excluded because the source was no longer significantly detected [4]. However, 3C 111 is very likely to be variable [5] and therefore no longer detectable in the second year. This has also been confirmed by Kataoka et al. [18], who find a significance $>5\sigma$ for 3C 111 using 24 months of *Fermi*/LAT data.

Since 3C 111 has been detected by *CGRO*/EGRET and *Fermi*/LAT at different epochs we assume that the source is a variable γ-ray emitter. We included data from the first *Fermi*/LAT catalogue where the source has been detected significantly. Our analysis gives a power law index that is similar to that given in the first catalogue, and the flux level is comparable [3].

Abdo et al. [2] have modeled the SED of the core of the radio galaxy Cen A, using simultaneous data from the radio regime up to the γ-regime, applying a single-zone SSC. Comparing the parameters for this model and our own (see Table 2) it is obvious that the models have significantly different parameter values. The magnetic field has a much higher value in the case of Cen A ($B = 6.2\,\mathrm{G}$), compared to the value we found for 3C 111 ($B = 0.04\,\mathrm{G}$). The higher magnetic field increases the resulting flux because the synchrotron power is dependent on the magnetic field. Contrarily, the Doppler factor used to model Cen A is low ($\delta = 1$) compared to the value we found for 3C 111, $\delta = 13.9$. A lower Doppler factor means that the emission is less boosted and therefore appear less energetic. There is also an order of magnitude difference between the radii of the emission volume, for Cen A $R = 3 \times 10^{15}\,\mathrm{cm}$ was used whereas we found $R = 2 \times 10^{16}\,\mathrm{cm}$ for 3C 111. Since this sets the amount of particles this also causes the flux to be lower for Cen A than for 3C 111. The higher value used for the magnetic field is attenuated by the lower Doppler factor and radius for Cen A, which causes the overall output to be lower, as expected for the less luminous sources.

Błażejowski et al. [9] used the Krawcynski code, which we also used, to model the high-energy peaked BL Lac object Mrk 421, using just an SSC component (no additional external Compton was needed). The parameter values they derived are in Table 2. Both the Doppler factor ($\delta = 10$) and the emitting region radius ($R = 7 \times 10^{15}\,\mathrm{cm}$) chosen for Mrk 421 are smaller than those chosen for 3C 111, but are larger than those of Cen A. Similar to Cen A, the magnetic field value for Mrk 421, $B = 0.405\,\mathrm{G}$, is larger than for 3C 111. The smaller radius and Doppler factor decrease the flux, but due to the choice of the magnetic field the flux in the SED for Mrk 421 is higher than the flux of 3C 111.

We conclude that the overall emission from 3C 111 can be modeled with a simple synchrotron self-Compton model, where no additional thermal Compton component is needed. Since the source is variable, simultaneous data would be needed to create the SED, which is not feasible because of

the different sensitivities of the instruments.
Earlier work [10] has shown that the X-ray spectrum of 3C 111 is of thermal inverse Compton origin, based on a correlation between the optical and X-ray flux, as well as a weak optical polarization and a smaller variance of the optical compared to the X-ray flux at shorter timescales. This is consistent with a reprocessing model where the X-rays are mostly produced by inverse Compton scattering of thermal optical/UV seed photons from the accretion disk. The X-ray spectrum of 3C 111 does show thermal components: the cut-off energy, reflection and the iron line, indicating a thermal IC component is significant in the X-ray regime. However, since we can model the overall SED with a non-thermal SSC model, we favour a hybrid model to explain both the thermal components (the high-energy cut-off, presence of an iron line and reflection) and the non-thermal components (an extra thermal component to model the entire SED is not required) of the overall emission. More data, especially in X- and γ-rays, will help strengthening such a hybrid model by disentangling the two components.

References

[1] Abdo, A. A., Ackermann, M., Ajello, M. et al. 2010, ApJ, 720, 912

[2] Abdo, A. A., Ackermann, M., Ajello, M. et al. 2010, ApJ, 719, 1433

[3] Abdo, A. A., Ackermann, M., Ajello, M. et al. 2010, ApJS, 188, 405

[4] Abdo, A. A., Ackermann, M., Ajello, M. et al. 2011, ArXiv:1108.1435

[5] Ackermann, M., Ajello, M., Allafort, A. et al. 2011, ApJ, 743, 171

[6] Ballo, L., Braito, V., Reeves, J. N., et al. 2011, MNRAS, 418, 2367

[7] Beckmann, V., Soldi, S., Ricci, C., et al. 2009, A&A, 505,417

[8] Beckmann, V., Jean, P., Lubiński, P., et al. 2011, A&A, 531, 70

[9] Błażejowski, M., Blaylock, G. Bond, I. H., et al. 2005, ApJ, 630, 130

[10] Chatterjee, R., Marscher, A. P., Jorstad, S. G., et al. 2011 ApJ, 734, 43

[11] Dadina, M. 2007, A&A, 461, 1209

[12] Dadina, M. 2008, A&A, 485, 417

[13] Hartman, R. C., Bertsch, D. L., Bloom, S. D., et al. 1999, ApJS, 123, 79

[14] Hartman, R. C., Kadler, M. & Tueller, J. 2008, ApJ, 688, 852

[15] Jorstad, S. G., Marscher, A. P., Lister, M. L., et al. 2005, AJ, 130, 1418

[16] Lichti, G. G., Bottacini, E., Ajello, M., et al. 2008, A&A, 486, 721

[17] Linfield, R. & Perley, R. 1984, ApJ, 279, 60

[18] Kataoka, J., Stawarz, Ł., Takahashi, Y., et al. 2011, ApJ, 740, 29

[19] Krawcynski, H., Hughes, S. B., Horan, D., et al. 2004, ApJ, 601, 151

[20] Molina, M., Bassini, L., Maliza, A., et al. 2009, MNRAS, 399, 1293

[21] Sguera, V., Bassani, L., Malizia, A., et al. 2005, A&A, 430,107